A&A 541, A79 (2012)
DOI: 10.1051/0004-6361/201118600

Astronomy & Astrophysics

The JCMT ^{12}CO(3–2) survey of the Cygnus X region

I. A pathfinder

M. Gottschalk[1,2], R. Kothes[1], H. E. Matthews[1], T. L. Landecker[1], and W. R. F. Dent[3]

[1] National Research Council of Canada, Herzberg Institute of Astrophysics, Dominion Radio Astrophysical Observatory, PO Box 248, Penticton, British Columbia, V2A 6J9, Canada
e-mail: roland.kothes@nrc.ca
[2] Department of Physics and Astronomy, University of British Columbia, 6224 Agricultural Road, Vancouver, British Columbia, V6T 1Z1, Canada
[3] ALMA SCO, Alonso de Cordova 3107, Vitacura, Santiago, Chile

Received 6 December 2011 / Accepted 19 January 2012

ABSTRACT

Context. Cygnus X is one of the most complex areas in the sky, rich in massive stars; Cyg OB2 (2600 stars, 120 O stars) and other OB associations lie within its boundaries. This complicates interpretation, but also creates the opportunity to investigate accretion into molecular clouds and many subsequent stages of star formation, all within one small field of view. Understanding large complexes like Cygnus X is the key to understanding the dominant role that massive star complexes play in galaxies across the Universe.
Aims. The main goal of this study is to establish feasibility of a high-resolution CO survey of the entire Cygnus X region by observing part of it as a pathfinder, and to evaluate the survey as a tool for investigating the star-formation process. We can investigate the mass accretion history of outflows, study interaction between star-forming regions and their cold environment, and examine triggered star formation around massive stars.
Methods. A $2^\circ \times 4^\circ$ area of the Cygnus X region has been mapped in the ^{12}CO(3–2) line at an angular resolution of 15″ and a velocity resolution of ~0.4 km s^{-1} using HARP-B and ACSIS on the *James Clerk Maxwell* Telescope. The star formation process is heavily connected to the life-cycle of the molecular material in the interstellar medium. The high critical density of the ^{12}CO(3–2) transition reveals clouds in key stages of molecule formation, and shows processes that turn a molecular cloud into a star.
Results. We observed ~15% of Cygnus X, and demonstrated that a full survey would be feasible and rewarding. We detected three distinct layers of ^{12}CO(3–2) emission, related to the Cygnus Rift (500–800 pc), to W75N (1–1.8 kpc), and to DR 21 (1.5–2.5 kpc). Within the Cygnus Rift, H I self-absorption features are tightly correlated with faint diffuse CO emission, while HISA features in the DR 21 layer are mostly unrelated to any CO emission. 47 molecular outflows were detected in the pathfinder, 27 of them previously unknown. Sequentially triggered star formation is a widespread phenomenon.

Key words. ISM: clouds – stars: formation – ISM: jets and outflows – surveys – HII regions – molecular data

1. Introduction

Star formation is the process that builds galaxies, and the formation of massive stars is the dominant influence on their evolution: massive stars trigger the formation of further stars and rapidly enrich their environment through stellar winds and supernova explosions. In the Milky Way, W49A, Westerlund 1 and Cygnus X have been identified as sites where large clusters of massive stars have formed. W49A contains at least 100 O stars in four clusters (Alves & Homeier 2003) embedded in some 10^6 $M_\odot$ of molecular gas. Westerlund 1 has at least 200 cluster members (Clark et al. 2005) including a rich population of Wolf-Rayet stars and luminous blue variables. Cygnus X is equally a laboratory where we can study the formation of massive stars: the region Cyg OB2, originally classified as an OB association, is actually a very large star cluster that contains about 120 O stars (Knödlseder 2000, 2004) and is within the boundaries of Cygnus X at a distance of about 1.7 kpc. Other OB associations at similar distances, Cyg OB1, OB8, and OB9 lie within the Cygnus X boundary. Cygnus X is relatively nearby, much closer than Westerlund 1 (3.9 kpc – Kothes & Dougherty 2007) or W49A (11.4 kpc – Alves & Homeier 2003). The mass of molecular gas in Cygnus X is estimated to be $\sim 4.7 \times 10^6$ $M_\odot$ (Schneider et al. 2006) assuming all the molecular gas is at the distance determined for Cyg OB2.

The study of Cygnus X as an entity is almost as old as radio astronomy itself. It was first recorded by Piddington & Minnett (1952) as an extended source in the vicinity of Cygnus A, an object of much interest at the time; the "X" denoted the extended nature of the source. These early measurements were made with an angular resolution of several degrees, but Piddington & Minnett (1952) determined a size for the source that matches modern estimates and also correctly deduced the thermal nature of the radio emission. With gradually improving angular resolution, the extended source broke up into sub-components. For example, Downes & Rinehart (1966) identified 26 discrete sources within Cygnus X with a 10.8′ beam. Eventually arcminute resolution was reached, 2.6′ at 4.8 GHz (Wendker 1984), 4′ at 408 MHz (Wendker et al. 1991), and 1′ in the Canadian Galactic Plane Survey at 1420 MHz (Taylor et al. 2003).

Optical obscuration is high in this direction, because Cygnus X lies partly behind the Cygnus Rift (at ~700 pc). Radio observations, of course, reveal the individual objects behind this obscuration, but compress the "bewildering amount of detail" (Wendker 1984) into a two-dimensional image. Observations of

radio spectral lines associated with various Cygnus X objects – e.g. Piepenbrink & Wendker (1988) – give a variety of systemic velocities, the most negative implying distances up to 4 kpc. Unfortunately kinematic distances within 2 or 3 kpc are unreliable in this direction because the radial velocity gradient is near zero, considerably smaller than the typical velocity dispersion of the gas. All that can be said is that there are many local objects in Cygnus X, as well as others at larger distances corresponding to the Perseus arm and even the Outer arm. Since this direction corresponds to the line of sight along the local arm, the Orion spur, the suggestion naturally arose that the apparent complexity and large amount of ionized gas are the simple consequence of viewing the Local arm end-on (Wendker et al. 1991).

The infrared waveband provided another window through the obscuration, and the improving technology of IR imaging yielded new information. Knödlseder (2000) used 2MASS data to demonstrate that the Cyg OB2 association is much larger than previously believed, containing about 2600 OB stars. This discovery suggested a much greater concentration of Cygnus X around the distance of Cyg OB2 at 1.7 kpc, and not stretched out along the Local arm. Knödlseder (2004) provides a comprehensive review of the Cygnus X region based on multi-wavelength data.

We now cross another technological boundary. In this paper we present observations of part of the Cygnus X region with an angular resolution of 15″ in the ^{12}CO(3–2) line using the HARP/ACSIS multi-beam system on the JCMT. We surpass the angular resolution of the earlier comprehensive line survey of Schneider et al. (2006) by a factor of 12. Our observations are a pathfinder for a survey in the ^{12}CO(3–2) line that could effectively and systematically map molecular clouds and diffuse emission in this entire region, revealing the dynamical relationship of various objects, with sufficient angular resolution to be able to discern the detailed structure of individual objects and complexes. Our effective physical resolution is 0.1 pc at a distance of 1.7 kpc.

This paper presents the data obtained from the pathfinder observations and gives some examples of the types of objects that can be studied and the types of questions that could be answered using the ^{12}CO(3–2) line, but does not include an exhaustive discussion of any single process. Subsequent papers will incorporate further observations and will more thoroughly discuss individual processes and objects.

2. Specific objectives of the JCMT Cygnus X ^{12}CO(3–2) survey

Cygnus X contains hundreds of H II regions, IRAS point sources, stellar clusters and OB associations as well as multiple objects with very bright radio emission. Here we can probe, within a small field of view, a major part of the cycle of star formation, a process that is strongly connected to the life-cycle of the molecular material in the interstellar medium (ISM). We can begin a study of the condensation of atoms into molecules, the transformation of dense molecular cloud cores into protostellar objects, the impact of newly formed and evolved stars on the surrounding interstellar medium, and, possibly, the triggering of another round of star formation.

Gibson et al. (2005) investigated H I self absorption (HISA) features using data from the Canadian Galactic Plane Survey (CGPS, Taylor et al. 2003). HISA clouds often have no CO counterparts, and Gibson et al. (2005) conclude that these clouds trace atomic gas on the path to formation of molecular hydrogen where CO molecules have not yet formed. With our high sensitivity and resolution we can probe HISA features for CO emission. We will eventually have a complete sample inside a very large molecular cloud and star formation complex, and we will be able to quantify the HISA-CO relation by comparing relative abundances of each species. Models of molecule formation rates, such as those of Glover et al. (2010), can determine ages, and give us deeper insights into the molecule formation process.

Among the many objectives of such a survey is the study of molecular outflows; the gravitational collapse of a molecular cloud ejects material in bipolar jets, and the discovery of a bipolar outflow, along with a dusty disk or envelope, signifies the presence of a protostar. Studies of outflows provide a fossil record (Bally et al. 2007) of the mass accretion. Lada (1985) outlined a method for calculating dynamical timescales assuming an average velocity over the lifetime and analyzing the spatial extent of the lobes. This analysis requires high angular resolution. For CO-HISA clouds containing outflows we can compare the outflow's dynamical timescale to the molecule formation timescale, determining star forming efficiency. ^{12}CO(3–2) line observations can provide basic outflow parameters. The high critical density of ^{12}CO(3–2) makes it an excellent tracer of dense material and line observations with the JCMT are probably the most sensitive probe of the warm outflow gas. Previous outflow searches have been biased toward near-infrared signposts of star formation. It is therefore of vital importance to make an unbiased and complete search for molecular outflows in a large molecular cloud and star formation complex such as the Cygnus X region.

Cometary nebulae are common within the Cygnus X region. Most of the cometary clouds should contain protostars, which are starbearing evaporated gas globules (EGGs). Most of the O and B stars within Cygnus X belong to OB associations such as Cyg OB2 (Knödlseder 2000) or related clusters (Le Duigou & Knödlseder 2002). A complete sample of EGGs with velocity information will allow us to explore the conditions for triggered star formation and determine whether evaporation around the protostar is stunting the growth of what would have been massive stellar objects. Schneider et al. (2006) proposed that nearly all molecular clouds in Cygnus X form groups that are dynamically connected, and that most of the Cygnus X objects are located at the distance of the Cyg OB2 cluster, 1.7 kpc. Unveiling the sequence of star formation and the entire evolutionary path of the Cygnus-X population will test the Schneider et al. postulate; to fulfill this aim we have to observe the entire Cygnus-X region at sub-arcminute angular resolution.

3. Pathfinder observations and data reduction

The observations for the Cygnus X pathfinder were carried out using the heterodyne array receiver system (Buckle et al. 2009) on the *James Clerk Maxwell* Telescope (JCMT), Mauna Kea, Hawaii. This system is composed of the 16-pixel array, HARP-B, as the frontend receiver and the ACSIS digital autocorrelation spectrometer as the backend correlator system. The observations were centered on the 345.7959 GHz line of the ^{12}CO(J = 3–2) transition in single-sideband mode with a total bandwidth of 1000 MHz and a channel spacing of 0.488 MHz. This resulted in 2048 channels with a channel spacing of 0.423 km s^{-1} and a total velocity coverage of about 850 km s^{-1}. The individual beams of the HARP receiver have half width of 15″ (FWHM), and the beams are spaced 30″ apart on a 4 × 4 grid. The data were obtained using the fast-raster scanning mode resulting in 7.5″ sampling in the scanning direction. For this purpose the 4 × 4 array is rotated so that the 16 receptors project scans onto

Table 1. Centre positions, dates of observation, and final sensitivity of the eight Cygnus X fields observed for the pathfinder.

Field	RA(J2000)	Dec(J2000)	Dates (YYYYMMDD)			Noise [mK]
1	$20^h25^m43.7^s$	41°54′44″		20070820		500
2	$20^h25^m40.9^s$	42°54′42″		20070819		850
3	$20^h31^m05.9^s$	41°54′44″		20070819		850
4	$20^h31^m08.2^s$	42°54′42″		20070728		750
5	$20^h36^m28.1^s$	41°54′44″	20090714	20100716	20100802	300
6	$20^h36^m35.5^s$	42°54′42″	20100717	20100718	20100802	250
7	$20^h41^m50.3^s$	41°54′44″		20100803		300
8	$20^h42^m02.8^s$	42°54′42″		20100725		300

the sky which are 7.5″ apart. During all of the observations one or two array elements were out of commission or missing, resulting in gaps in the raw data cubes. To compensate more easily for the missing receptors individual scans were separated by half an array.

The final data cube is centered on α(J2000) = 20^h34^m and δ(J2000) = 42°26′ and is a mosaic of eight smaller fields, each about one square degree in size. The location of those fields within the Cygnus X region is displayed in Fig. 1 and their characteristics are summarized in Table 1. The scanning speed of the telescope was 37.5″ per second with a 5 Hz sampling rate, completing each observation in around 90 min. All fields were scanned at least twice in a boustrophedon pattern, once along right ascension and once along declination, to reduce scanning effects. The observations took place in the period May to August 2007 for fields 1 to 4, July 2009 for field 5 and July to August 2010 for fields 5 to 8 (see Table 1). The fields were observed during varying grades of weather, a fact reflected in significant difference of sensitivity (see Table 1).

Each field was reduced according to the ACSIS DR workflow by using KAPPA, SMURF, CONVERT and GAIA from the STARLINK package. The full mosaic containing all the fields was assembled using MADR from the DRAO Export Software Package. The data were originally in the form of time-stamped streams of spectra for each detector. These time series were cleaned of any noisy spectral bounds, any bad/noisy receptors, and any spikes amongst the spectra. The cleaned raw data from each scanning direction were then combined into one data cube and analyzed simply, only to determine ranges free of emission lines for baseline correction. A second-order baseline was first fitted to the emission-line-free channels along the spectral axis and subtracted from the data cube.

Due to atmospheric condition and receiver instabilities, base levels of individual scans are not always constant. These "scanning effects" are a common feature of raster scanning. They were removed by using the unsharp masking technique as described in Sofue & Reich (1979). The assumption for this method is that the baseline variation along each scan is a smooth function and independent of its neighbours. For the pathfinder data we used a filter beam of 90″ × 30″ ($\Theta_{maj} \times \Theta_{min}$, where Θ_{maj} is the beam perpendicular to the scanning direction and Θ_{min} the beam parallel to it). The convolution of the original data set with this filter beam effectively smears out the scanning effects. Therefore a difference map of the smoothed data subtracted from the original data includes only information about the baseline error and structures smaller than the filter beam. The latter are distributed randomly around the smooth function representing the scanning effect. A polynomial of order 3 is then fitted to the difference data after subtracting all left-over emission above 5σ. The fitted baselines are then removed from the original dataset resulting in a "true" distribution of the ^{12}CO(3–2) emission.

Occasionally there were holes in the clean data cube where missing receptors on HARP overlapped from each scanning direction. These were interpolated using the KAPPA *fillbad* routine which averages the surrounding pixels. After combining the cubes for the different scanning directions a clean data cube for each field was obtained. The clean data cube was then ready to be combined with the other cubes to create the full mosaic.

Emission in the final data cube was contained in a region of 356 channels. To reduce its size, only these channels were included in the final data product. The resulting cube is ∼2° × 4°, with an angular resolution of 15″, and spans a velocity range of −100 to +50 km s^{-1}. Channels at velocities less than −100 km s^{-1} and greater than 50 km s^{-1} were inspected for emission of extragalactic origin, but none was found.

4. The pathfinder data

The observations were taken in two very distinct areas of the Cygnus X region. The western part of the pathfinder covers fields 1 through 4 (see Figs. 1–3), and represents a very "quiet" area largely free of dynamical activity. The eastern part covers fields 5 through 8 (see Figs. 1, 4, and 5) and contains a lot more activity in the form of H II regions and star forming cores, centered at the well-known complex related to DR 21. The pathfinder area was chosen this way to include both presumably active and less active areas of the Cygnus X region.

We found an astonishing richness in structure and brightness, from faint, diffuse clouds to dense cores at the resolution limit in both regions, the quiet western part and the more active eastern part. Each observed field is shown through a zeroth and first moment map in Figs. 2 to 5. The zeroth moment maps are created by integrating the brightness temperature T_b over the velocity range indicated in the figure captions: $\int T_b \, dv$. The first moment maps are created by averaging the velocity v of each spectrum weighted by its brightness temperature: $\frac{\int T_b \, v \, dv}{\int T_b \, dv}$. The zeroth moment maps display all the emission within the velocity range while the first moment maps illustrate the dominant velocity of the CO emission along each line of sight.

4.1. The western region

The western region (Figs. 2 and 3) contains considerably less ^{12}CO(3–2) emission than the eastern region, as can be seen in a comparison of Figs. 2 through 5. The bulk of the CO emission in this area seems to originate from molecular clouds associated with the H II region complex NGC 6914. Those can be found around 20^h25^m, 42°23′ in a velocity range from about 0 to +10 km s^{-1}. Within these clouds we detected four molecular outflows (see Table 2), all of which are accompanied by IRAS point sources indicating young protostars. The extended ^{12}CO(3–2)

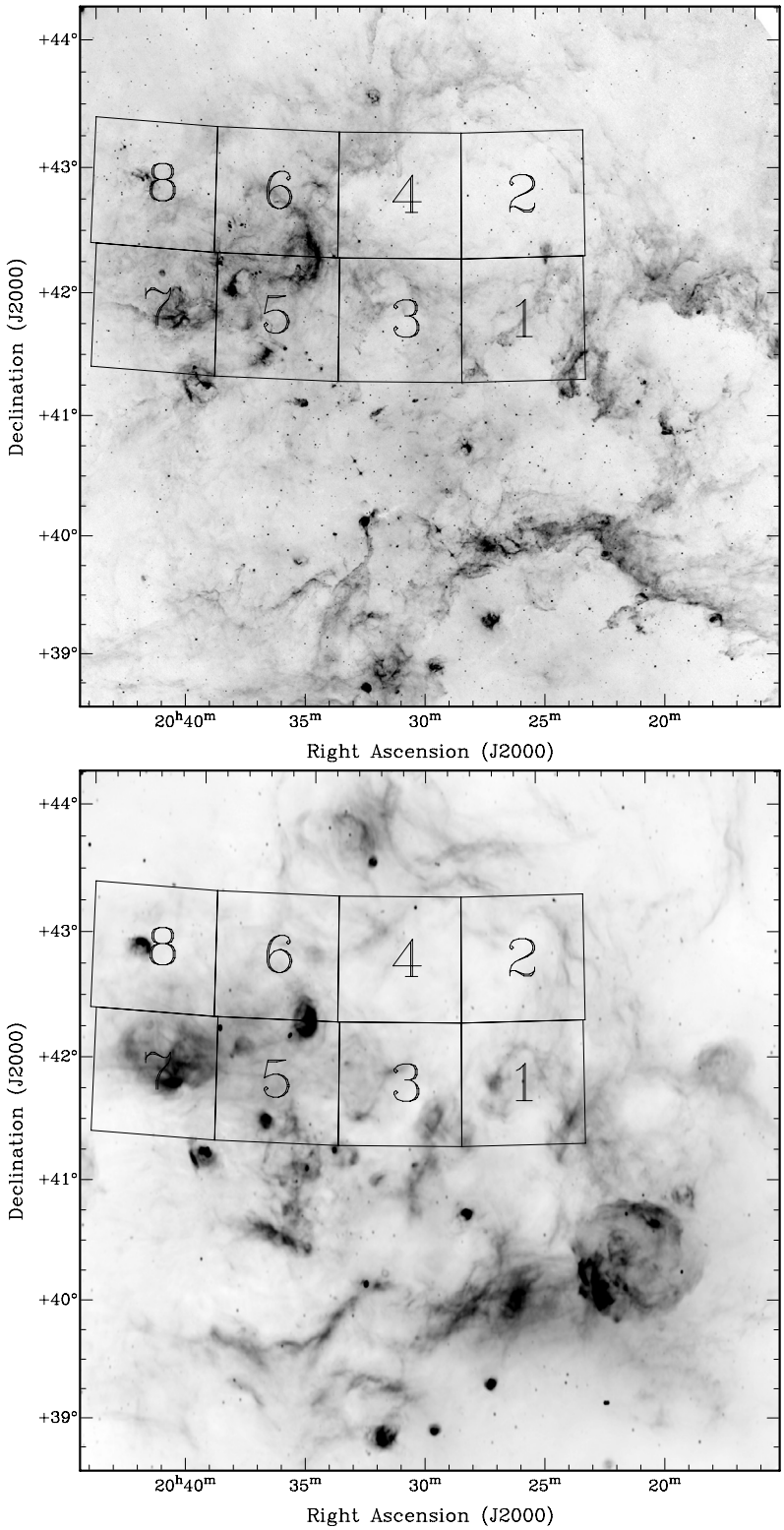

Fig. 1. The Cygnus X region as seen in the Midcourse Space Experiment (MSX) at 8 μ (*top*) and in the Canadian Galactic Plane Survey (Taylor et al. 2003) in total intensity at 1420 MHz (*bottom*). The location of the pathfinder area with its eight 1° × 1° fields is indicated.

emission coincides with a HISA complex discovered in data of the Canadian Galactic Plane Survey by Gibson et al. (2005). This diffuse cloud also completely absorbs the emission from the bipolar outflow related to IRAS 20227+4154 in the velocity range +4.5 to +6.4 km s^{-1} indicating a very large optical depth and so a high molecular column density for that cloud. This diffuse cloud must be a foreground object to IRAS 20227+4154, since it absorbs emission from both outflow lobes and therefore is probably unrelated.

Another source of considerable ^{12}CO(3–2) emission in the western region is a cometary shaped nebula with CO emission at low negative velocities (Fig. 3), visible at α(J2000): 20^{h}31^{m}11^{s} and δ(J2000) from 43°00′ to 43°15′. Two molecular outflows are found towards the dense core within this bright nebulous object.

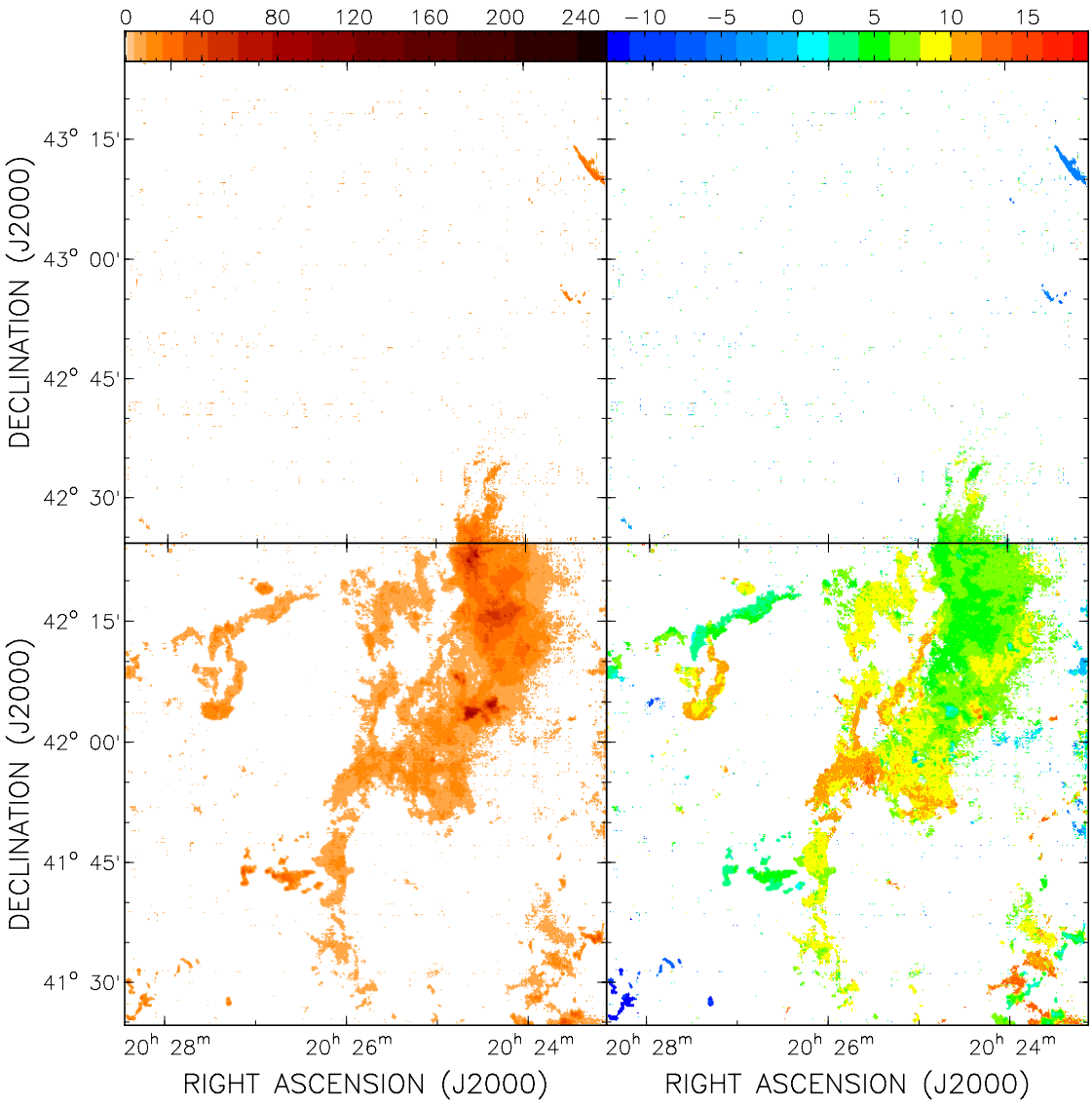

Fig. 2. Zeroth and first moment maps of field 1 (*bottom*) and field 2 (*top*). For the calculation of zeroth and first moment maps, please consult the text in Sect. 4. Both maps were integrated from −20 km s^{-1} to +30 km s^{-1}. Only velocities with a signal above 3σ were used in the integration. In the images only those pixels are displayed that have a signal above 3σ in at least 3 velocity channels. The zeroth and first moment maps are displayed in units of K km s^{-1} and km s^{-1}, respectively.

Both outflows were previously unknown. The position of these outflows corresponds to the location of IRAS 20294+4255 indicating that protostars are likely present. Due to the low resolution of the IRAS data it is not clear whether this IRAS source corresponds to one of the outflows or may be a combination of both.

In the north-east of the western region is another diffuse cloud of emission at low negative velocities (Fig. 3), which seems to be unrelated to the cometary feature. These clouds continue into the eastern region and seem to be part of the very large molecular cloud complex connected to DR 21. The relative lack of activity within this region is probably due to the absence of large H II regions, typically seen as radio bright DR or W objects, which have a pronounced effect on their surrounding ISM.

4.2. The eastern region

The eastern portion of the pathfinder is far more complex than the western region, as can be easily seen by comparing Figs. 2 to 5. There were major concerns that the Cygnus X region might be too crowded and complicated for a project like ours with many sources located along the line of sight, thus making physical interpretation of individual objects too difficult through projection effects and the ravages of ongoing star formation. Figures 4 and 5 seem at first glance to confirm that assessment. The eastern portion of our survey area was previously studied by Schneider et al. (2006) using the ^{12}CO(3–2) and ^{13}CO(2–1) & (3–2) lines with the KOSMA 3 m telescope. Their survey led them to believe that all the emission in velocity ranges −10 to +20 km s^{-1} is dynamically connected, which would greatly complicate interpretation.

However, in contrast to the study by Schneider et al. (2006), we detect three distinct layers of ^{12}CO(3–2) emission, which do not show any interconnection. The three layers can be seen clearly separated in the position-velocity diagrams in Fig. 6 (top panels). We also display RA–v and v–Dec images towards the well-known compact H II regions DR 21 (centre) and W 75 N (bottom) to show that even towards these busy and very dynamic

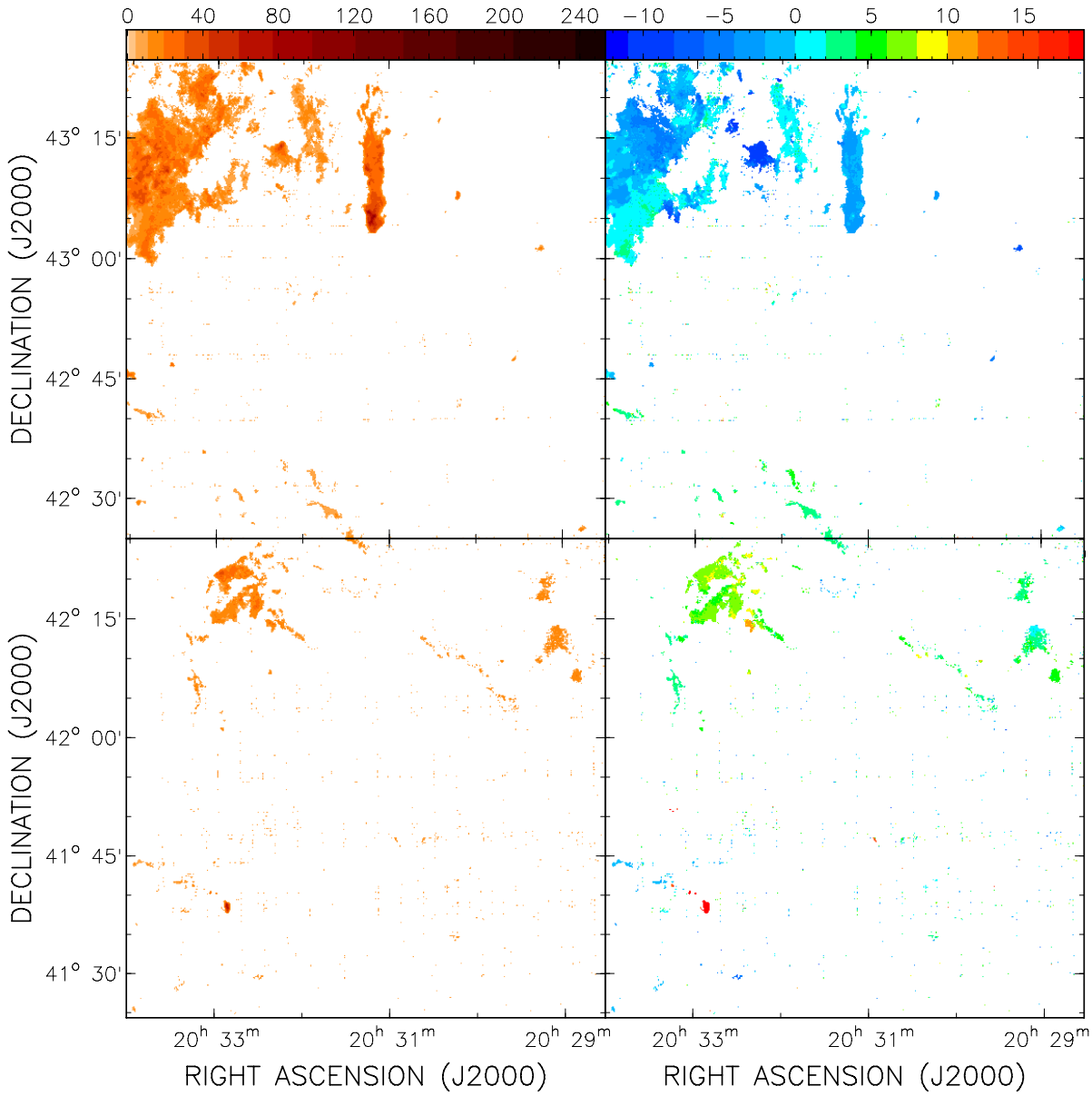

Fig. 3. Zeroth and first moment maps of field 3 (*bottom*) and field 4 (*top*). For the calculation of zeroth and first moment maps, please consult the text in Sect. 4. Field 3 was integrated from -12 km s^{-1} to $+25$ km s^{-1} and field 4 from -15 km s^{-1} to $+20$ km s^{-1}. In the images only those pixels are displayed that have a signal above 3σ in at least 3 velocity channels. The zeroth and first moment maps are displayed in units of K km s^{-1} and km s^{-1}, respectively.

regions individual features are separable in velocity space. The separation of the three layers is a direct result of the higher angular resolution of our data; earlier studies used poorer angular resolution, which smeared together objects that we now see to be spatially distinct.

Layer 1 in Fig. 6 is concentrated in radial velocities from ≈ -10 km s^{-1} to ≈ 0 km s^{-1}. This velocity range contains the H II region complex DR 21 and other H II regions and star formation regions connected to it. There is a significant amount of faint diffuse emission in layer 2 at low positive velocities that moves in like a curtain of fog, covering everything. All emission from objects that have their peak emission in the other velocity ranges, but still show some emission at low positive velocities (outflows or clouds with wide emission lines) is completely absorbed by these diffuse clouds. We believe that these clouds represent the Cygnus Rift, an area of dark clouds at a distance of 500 to 800 pc, responsible for a jump in visual extinction for stars observed in this direction (e.g. Schneider et al. 2006, and references therein). This is the first time that the molecular line emission of the rift has been separated from the emission of other molecular clouds in the area. Layer 3 of ^{12}CO(3–2) emission in Fig. 6 can be found above +8 km s^{-1}. This layer encompasses gas primarily connected with W 75 N and related H II regions and star formation complexes.

Mao et al. (2009) previously studied the possibility that DR 21 and W 75 N are two regions in collision. They concluded that the two regions overlap spatially, but not in velocity and are therefore not connected. We find similar results. The outflows from DR 21 and W 75 N clearly show absorption in their high velocity wings by the diffuse shroud between +7 and +8 km s^{-1}. Since the velocity of the emission in the wings is not at all an indication of its location, and since the bulk of emission

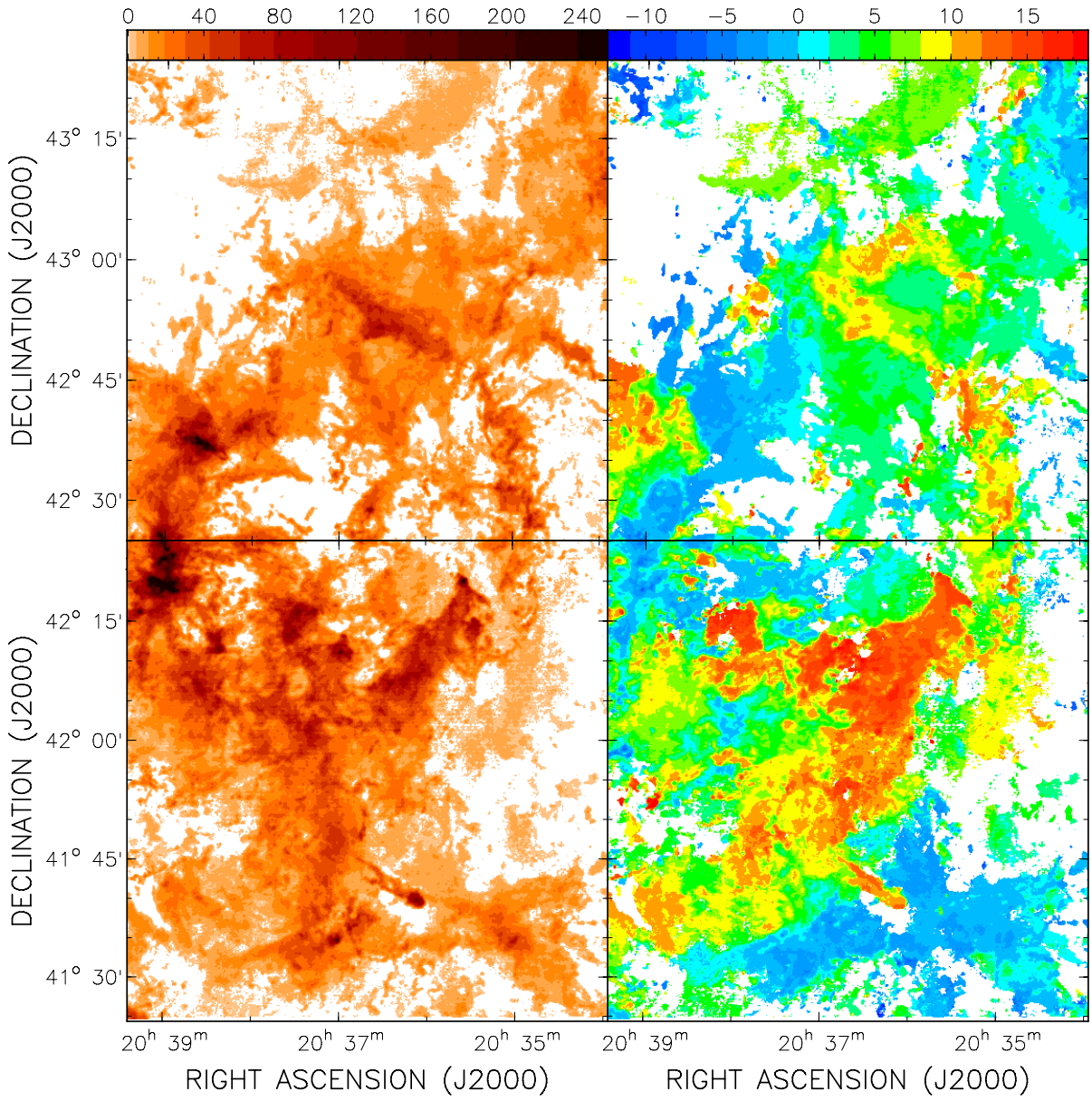

Fig. 4. Zeroth and first moment maps of field 5 (*bottom*) and field 6 (*top*). For the calculation of zeroth and first moment maps, please consult the text in Sect. 4. Both fields were integrated from −20 km s^{-1} to +30 km s^{-1}. In the images only those pixels are displayed that have a signal above 3σ in at least 3 velocity channels. The zeroth and first moment maps are displayed in units of K km s^{-1} and km s^{-1}, respectively.

from W 75 N is at a different velocity from the bulk of emission from DR 21, we find no evidence suggesting the two regions are colliding.

4.3. Kinematic distances

By using a flat rotation curve, with the IAU-supported values for the Galacto-centric distance of the Sun of $R_\odot$ = 8.5 kpc and its orbital velocity of $\Theta_\odot$ = 220 km s^{-1} we find that objects should be seen to a maximum radial velocity of around +4 km s^{-1}. Using other more modern values for $\Theta_\odot$ and $R_\odot$ lead to similar results. Based upon the new view of the Milky Way from Spitzer (Churchwell et al. 2009) the direction we are observing ($\ell \sim 80°$) looks through our local spiral arm, the Orion Spur, to a distance of about 2.5 kpc, through the Perseus arm, and finally through the Outer Arm. Objects at the maximum velocity of the rotation curve are those objects closest to the center of our Galaxy. We clearly find a lot of emission at velocities more positive than +4 km s^{-1} with multiple objects seen upwards of +20 km s^{-1}. This is beyond anything that can be explained by velocity dispersion.

Burton (1971) and Roberts (1972) showed that streaming motions caused by a spiral density wave pattern can systematically shift the bulk average motion of local gas into positive velocities in this part of our Galaxy, since we are located between major spiral arms, where streaming motions along the orbital direction is at its maximum. This could account for about +6 km s^{-1} (Wielen 1979) in our observations towards Cygnus X. Since there is still a high discrepancy in radial velocity the most likely scenario for the residual velocity is that these objects are being pushed away from us at high speeds, up to about 10 km s^{-1}. This clearly shows that traditional kinematic distance estimates in the pathfinder area cannot be trusted. The

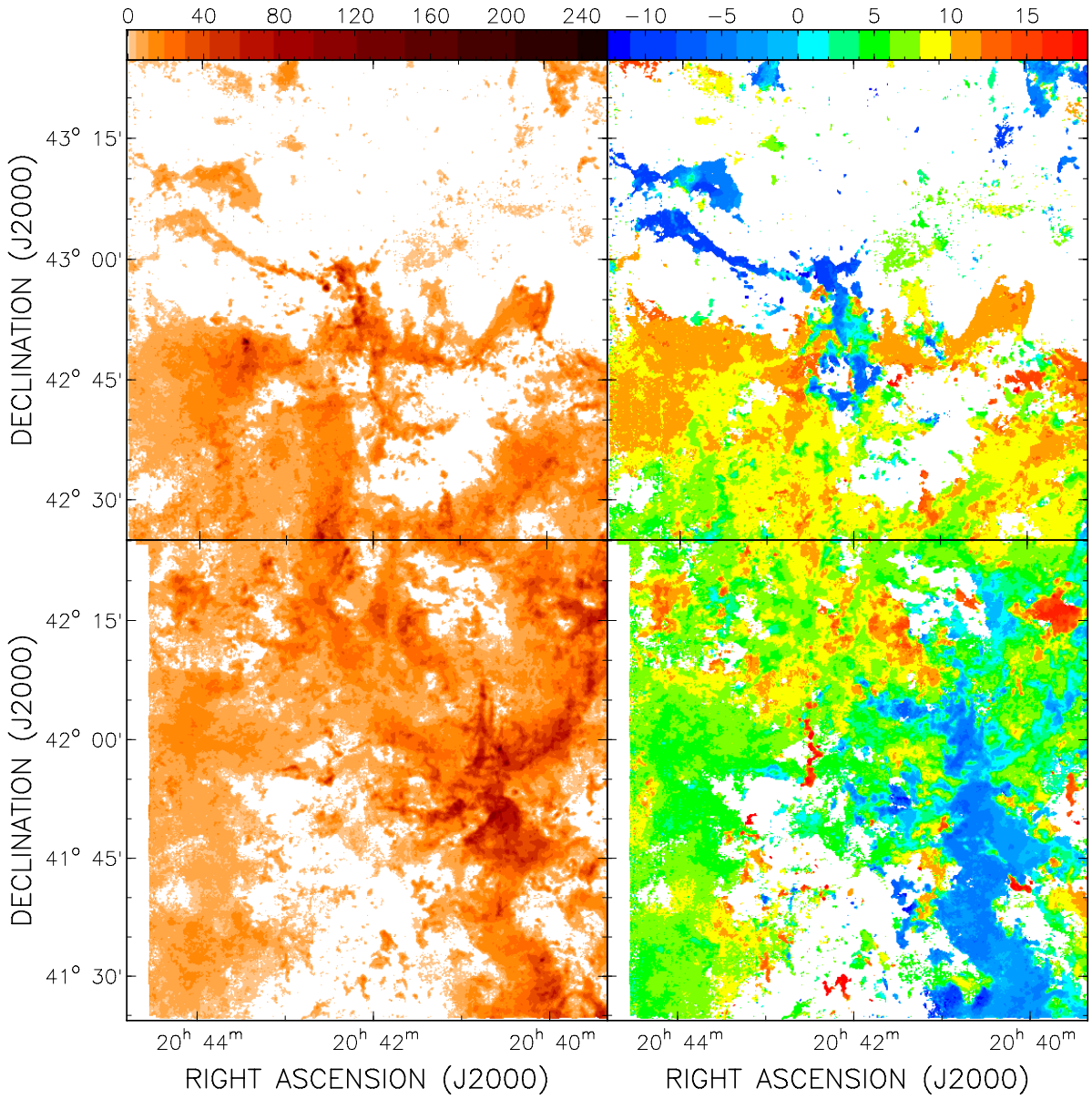

Fig. 5. Zeroth and first moment maps of field 7 (*bottom*) and field 8 (*top*). For the calculation of zeroth and first moment maps, please consult the text in Sect. 4. Field 7 was integrated from -18 km s^{-1} to $+25$ km s^{-1} and field 8 from -15 km s^{-1} to $+22$ km s^{-1}. In the images only those pixels are displayed that have a signal above 3σ in at least 3 velocity channels. The zeroth and first moment maps are displayed in units of K km s^{-1} and km s^{-1}, respectively.

main information to be gained from radial velocities is an object's position and dynamics relative to the large cloud complexes present in the area.

5. Discussion of the results from the pathfinder

In this section we make a brief analysis of the pathfinder data according to the different scientific objectives laid out in Sect. 2.

5.1. Cold molecular clouds, HISA, and the "Great Cygnus Rift"

Gibson et al. (2005) investigated H I self absorption features in the Galactic plane in the Outer Galaxy using data from the Canadian Galactic Plane Survey (Taylor et al. 2003). In their catalogue of major CGPS HISA features (Gibson et al. 2005, Table 1) all HISA in Cygnus X is listed as one major feature GHISA 079.88+0.62+02. This is by far the largest HISA feature in this catalogue, more than 4 times bigger than the second largest. It also shows the largest velocity coverage from about -10 km s^{-1} to $+15$ km s^{-1}. According to Gibson et al. (2005) most stronger HISA is organized into discrete complexes, many of which follow a longitude-velocity distribution that suggests that they have been made visible by the velocity reversal of the Perseus arm's spiral density wave. The cold H I revealed in this way may have recently passed through the spiral shock and be on its way to forming molecules and, eventually, new stars.

In the area of the Cygnus X pathfinder we find HISA in two of the three previously described layers of ^{12}CO(3–2) emission from ≈ -8 km s^{-1} to $\approx +10$ km s^{-1}. In layer 3 no significant HISA feature is detected. Layer 2 shows most of the significant HISA, which can be found in almost the entire pathfinder area. All of

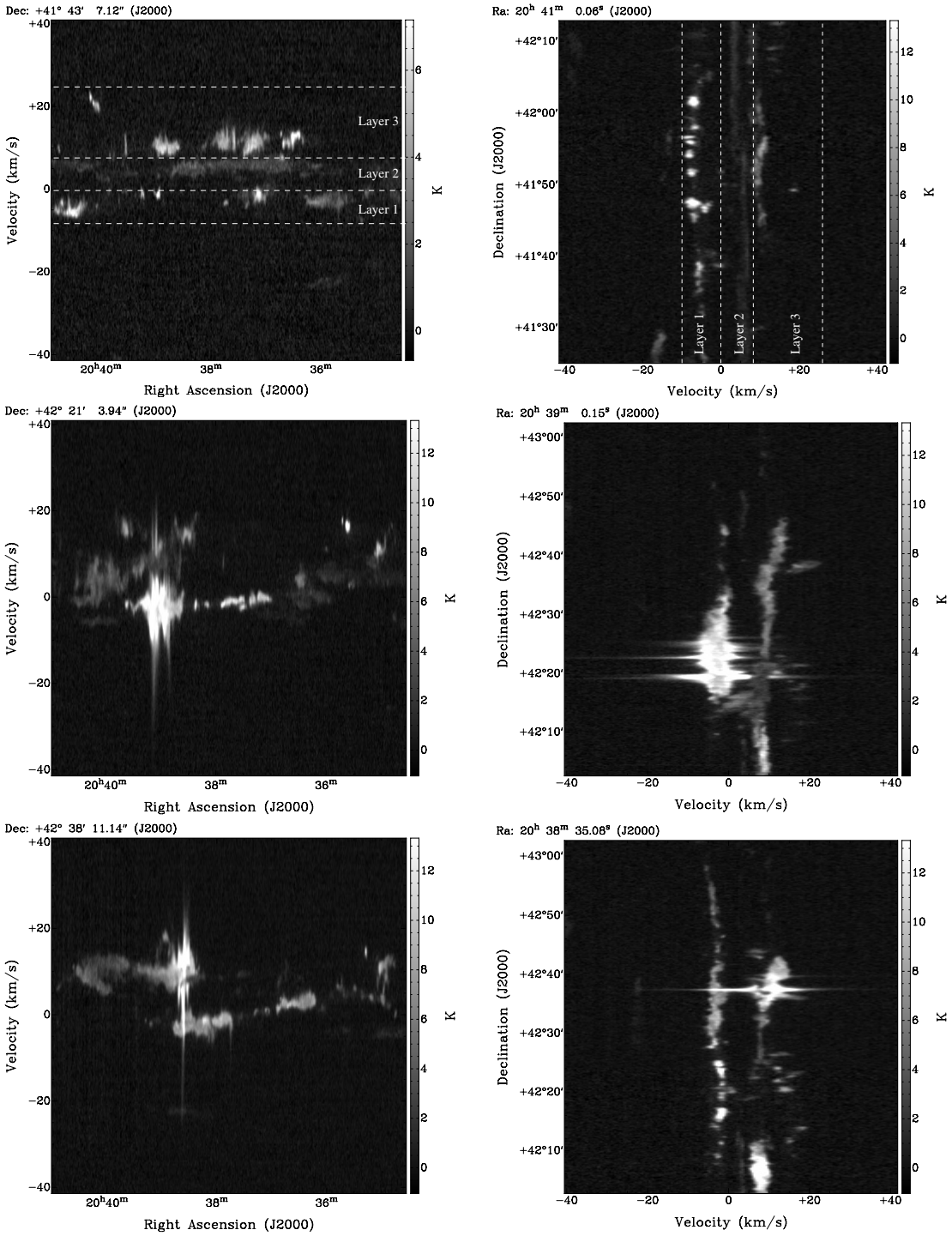

Fig. 6. Sample RA–v (*left*) and v–Dec (*right*) maps to demonstrate that the apparently very complex and chaotic appearance in the zeroth and first moment maps shown in Figs. 2 to 5 can easily be resolved in the third dimension. The two *top* panels represent an area where all three layers of ^{12}CO3–2 emission (see text) that we found in the pathfinder are visible, the centre panels were taken towards DR 21, and the *bottom* panels towards W 75 N.

these features seem to be related to large and diffuse ^{12}CO(3–2) emission clouds of very low surface brightness. These clouds must be tremendously dense and cold, because they have, in addition to the low surface brightness, very small line width and completely absorb all the emission from background clouds that reaches into their velocity range. One example is shown in the upper panel of Fig. 7.

Layer 1 also shows a lot of complex HISA, in particular in the eastern area, but also in the upper part of the western region. But most of the HISA in this velocity range does not correspond to any ^{12}CO(3–2) emission in the pathfinder. In Fig. 7 (lower panels) we display an example of a very bright molecular cloud connected to the DR 21 complex that does correspond to a HISA complex with very deep absorption.

Before analysing the detected HISA features and their corresponding molecular clouds we need to discuss briefly under what circumstances HISA is seen. The most important characteristic of HISA is that two separate H I clouds along the line

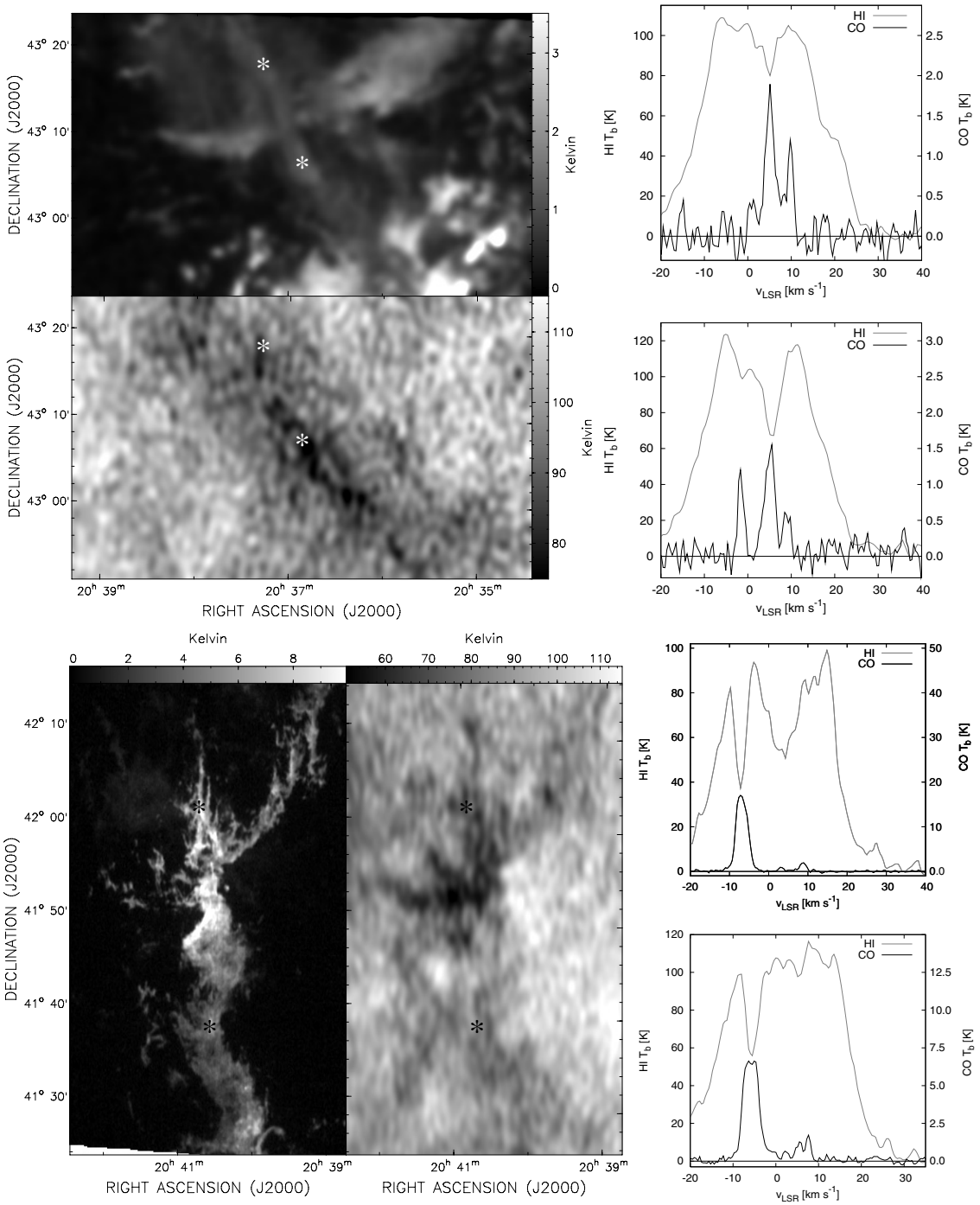

Fig. 7. Two examples of clouds of ^{12}CO(3–2) emission that coincide with extended features of H I self absorption. In the *left* ^{12}CO(3–2) emission maps are shown with corresponding H I images. On the *right* CO and H I profiles are displayed. These were taken at the positions marked with the asterisks in the images. In the *top* we show an example for a Cygnus Rift cloud at a velocity of +5 km s^{-1}. The *bottom* represents a cloud at low negative velocities connected to DR 21. The images represent a velocity of −8 km s^{-1}.

of sight with overlapping radial velocity are needed. The background cloud must be a warm H I cloud of high radio surface brightness while the foreground cloud – the absorbing cloud – must be cold and of high optical depth implying a high density. In addition the amplitude of the absorbed signal must be higher than the emission of the absorbing cloud. In the Canadian Galactic Plane Survey most of the HISA features are found in the Perseus arm where the cold foreground gas is located in the spiral shock and the warm background is interarm gas from beyond the Perseus arm (Gibson et al. 2005).

Another typical location for HISA would be the inner Galaxy where the differential Galactic rotation produces a distance ambiguity for any given radial velocity from our point of view. Towards the Cygnus X region the line of sight passes through the inner Galaxy and returns to the Sun's galactocentric radius at a distance of about 3.0 kpc, assuming the IAU endorsed value for $R_\odot$. This is much farther than any significant object in the Cygnus X region is believed to be. This implies that all molecular clouds in Cygnus X should be found within a radial velocity range of ≈0 km s^{-1} to ≈+10 km s^{-1} based entirely on their orbital

motion around the Galactic centre (see discussion in Sect. 4.3). Any clouds with radial velocities outside that range must have been either pushed away from or towards us by stellar winds or supernova shock waves.

Under these circumstances it is not surprising that we do not find HISA corresponding to the ^{12}CO(3–2) emission layer 3. In particular radial velocities in excess of +20 km s^{-1} are highly forbidden in view of Galactic rotation models. The only way that clouds can have received such a high positive radial velocity is that some force has pushed them away from us. It would be very unlikely that this has happened twice at separate distances along the line of sight with a warm cloud being pushed away with just exactly the velocity needed to be the background for a cold cloud that is pushed away from us too. This does not mean that there are no cold dense H I clouds present. We just do not have the bright background to reveal them in self absorption.

The HISA features related to low surface brightness molecular clouds in layer 2 are a typical result of the inner Galaxy distance ambiguity and can be easily explained by a flat rotation curve combined with density wave streaming motion (see Sect. 4.3). In this case the cold and dense absorbing clouds must be located between the Sun and the tangent point at about 1.5 kpc (the location closest to the Galactic center) and the warm background gas must have a distance between 1.5 and 3.0 kpc. The most likely explanation for the large amount of cold atomic and molecular gas together is that this layer of ^{12}CO(3–2) emission represents the Great Cygnus Rift, a large molecular cloud and dust complex that reveals itself by a large jump in observed visual extinction of stars at a distance of about 500 to 800 pc (Schneider et al. 2006, and references therein). There is a lot of evidence to support this explanation. The molecular gas and HISA observed in this velocity range can be found almost everywhere over the mapped region and the observed radial velocity indicates a location closer than 1.5 kpc. The atomic and molecular gas must be very cold and very dense, as evidenced by the deep absorption signals these clouds cause. These same clouds seem to be related to smooth dust emission seen in the 8μ maps of the MSX survey (although the Cygnus X area is so complex that a positive identification cannot be made). This likely combination of intermixed cold dust, atomic and molecular gas represents the perfect environment for the formation of molecules. This would be the first time that the molecular gas related to the Cygnus Rift has been separated from other clouds in velocity space.

The HISA features related to layer 1 are not as easily explained. A flat rotation curve combined with density wave streaming motion does not account for a distance ambiguity for gas at negative velocities in the direction of Cygnus X. This can be explained by assuming that the warm background H I clouds are the ones predicted by Galactic rotation models, which would locate them at a distance of about 3 to 4 kpc, an interarm location between the local arm and Perseus arm. The foreground cold and dense absorbing clouds must have been pushed towards us by an external force like stellar winds or supernova shock waves. This would imply a distance smaller than 3 kpc.

It is interesting to note, that within the Cygnus Rift, literally every HISA feature is accompanied by a detectable molecular cloud, while most of the HISA at low negative velocities does not correlate with ^{12}CO(3–2) emission. In the Canadian Galactic Plane Survey HISA clouds often have no CO counterparts, and Gibson et al. (2005) conclude that these clouds trace atomic gas on the path to formation of molecular hydrogen where CO molecules have not yet formed. This could indicate that most of the dense clouds at low negative velocities are in an earlier phase of the molecule formation process, while the clouds of the Cygnus Rift are further developed. However, a contrary indication would be the fact that in layer 1 more star formation, as revealed by molecular outflows, is found than in the Cygnus Rift, indicating that the Cygnus Rift clouds had less time yet to develop gravitational instabilities and collapse. On the other hand, outflows naturally are only found to be connected to HISA, which are related to observable molecular clouds. The Cygnus Rift may represent just a snapshot in the evolutionary path of molecule formation, while layer 1 represents a large spread along that evolutionary path. Clearly observations over a wider area are required to make a more thorough investigation of the evolutionary state of the molecule formation process in Cygnus X.

5.2. Molecular outflows

The presence of a bipolar outflow, together with a dusty disk and envelope, signifies the presence of a protostar. The outflow mechanism is believed to be an energetic mass-ejection phenomenon associated with mass accretion in the very early stages of stellar evolution. It is most energetic at the earliest Class 0 and 1 phases of proto-stellar development. The high critical density of ^{12}CO(3–2) makes it an excellent tracer of dense material and line observations with the JCMT are probably the most sensitive method of detecting the warm outflow gas (Dent et al. 2009). Previous outflow searches have generally been biased toward near-infrared signposts of star formation. It is therefore of vital importance to make a complete and unbiased search for molecular outflows in a large molecular cloud and star formation complex such as the Cygnus X region.

The outflowing mass initially leaves the protostar with speeds several times the escape speed (several $\times$100 km s^{-1}), but collides with the local parent cloud slowing the jet down and creating shocks and gas velocities of a few $\times$10 km s^{-1} (Stahler & Palla 2005). Depending on the density and thickness of the parent cloud an outflow will pierce through the local ISM or it will be slowed down eventually to the velocity of the local ISM. By examining the spectra of the outflow a basic understanding of the outflow's history can be ascertained. This is done by studying the evolution of the outflow over velocity.

We searched the whole data cube by eye, examining it in RA $\times$ v and v $\times$ Dec slices. High velocity wings are readily seen stretching away from the core along the velocity axis. Examples can be seen in Fig. 6 (lower two panels). We include any source with a spectrum containing a width at its base of over 8 km s^{-1} that is clearly non-Gaussian in shape. Towards a few of the outflows other objects can be seen contaminating the spectra (i.e. they appear to lengthen the wings, or cause another peak off the central velocity), so a careful analysis of the cube in RA $\times$ Dec $\times$ v needs to be carried out. This contamination often arises from extended emission that covers the area, or from small dense clouds overlapping spatially with some part of the outflow.

We found 47 outflows (listed in Table 2) in the ^{12}CO(3–2) data cube of the pathfinder with 27 of them being new discoveries. The very complex multi-outflow cores related to DR 21 and W 75 N are counted as one outflow each in our list. 46 of these outflows fall within the velocity range of the Cygnus X region and of them – G80.314+1.330 – is likely a Perseus arm object with a radial velocity of about $-$31 km s^{-1}. To the best of our knowledge, within our observed survey area we have detected all previously confirmed molecular outflows that were detected in CO observations.

Table 2. A list of outflows detected in the pathfinder.

Identifier	α [h m s]	δ [° ′ ″]	$v_{\rm lsr}$ [km s^{-1}]	Infrared source
G79.886+2.552	20 24 31.6	42 04 20	6.6	IRAS 20227+4154
G80.158+2.727	20 24 35.7	42 23 41	6.0	IRAS 20228+4215
G80.149+2.710	20 24 38.6	42 22 42	6.0	2MASS J20243430+4221265
G79.962+2.556	20 24 44.7	42 08 11	5.5	IRAS 20231+4157
G81.424+2.140	20 31 12.3	43 04 53	−1.7	IRAS 20294+4255
G80.314+1.330	20 31 12.3	41 42 30	−31.4	2MASS J20311521+4142249
G81.435+2.147	20 31 12.5	43 05 42	−2.4	IRAS 20294+4255
G81.302+1.055	20 35 33.5	42 20 17	14.6	2MASS J20353805+4220318
G80.815+0.661	20 35 40.9	41 42 44	−3.0	2MASS J20352935+4143345
G80.972+0.700	20 36 01.2	41 51 41	6.0	IRAS 20342+4139
G81.218+0.877	20 36 03.3	42 09 50	13.6	
G80.832+0.570	20 36 07.6	41 40 15	11.5	IRAS 20343+4129
G81.140+0.687	20 36 37.2	41 59 16	12.3	
G81.539+0.983	20 36 38.5	42 29 02	2.6	
G81.829+1.195	20 36 40.2	42 50 35	13.6	
G80.866+0.415	20 36 53.6	41 36 17	−4.7	IRAS 20350+4126
G81.365+0.781	20 36 56.7	42 13 26	16.6	
G81.340+0.755	20 36 58.6	42 11 17	15.7	2MASS J20365781+4211303
G80.862+0.385	20 37 00.6	41 35 00	−1.4	IRAS 20352+4124
G81.437+0.728	20 37 24.5	42 14 57	−1.3	MSX6C G081.4515+00.7280
G80.916+0.331	20 37 25.0	41 35 39	−1.3	IRAS 20355+4124
G81.460+0.735	20 37 27.3	42 16 19	−1.3	2MASS J20372634+4215518
G81.462+0.736	20 37 27.3	42 16 27	17.4	
G81.794+0.910	20 37 47.6	42 38 37	−0.4	2MASS J20374746+4238370
G81.861+0.959	20 37 48.0	42 43 35	−0.8	
G81.813+0.919	20 37 49.1	42 39 51	−0.8	2MASS J20374733+4240529
G81.770+0.851	20 37 58.3	42 35 19	−0.4	
G81.857+0.905	20 38 01.4	42 41 25	−3.0	2MASS J20375536+4240468
G81.831+0.880	20 38 02.6	42 39 17	−2.1	2MASS J20380710+4238521
G81.634+0.726	20 38 03.7	42 24 18	8.5	
G81.867+0.780	20 38 35.9	42 37 22	10.6	W75N
G81.773+0.687	20 38 41.3	42 29 28	−3.8	[CGC93] FIR 11
G81.681+0.540	20 39 01.1	42 19 43	−3.0	DR21
G81.663+0.468	20 39 15.9	42 16 15	19.9	2MASS J20391672+4216090
G81.117-0.140	20 40 04.1	41 28 03	−4.2	MSX6C G081.1225-00.1343
G81.175-0.100	20 40 05.1	41 32 15	−3.8	
G81.559+0.183	20 40 08.6	42 00 52	9.3	
G81.551+0.098	20 40 28.7	41 57 21	−5.9	
G81.450+0.016	20 40 29.7	41 49 35	−4.7	
G81.582+0.104	20 40 33.3	41 59 05	−5.9	2MASS J20403814+4200055
G81.476+0.020	20 40 33.8	41 50 56	−4.7	
G81.317-0.103	20 40 33.9	41 38 53	−5.1	HFE 69
G81.632+0.102	20 40 43.7	42 01 21	−6.8	
G82.186+0.105	20 42 33.1	42 27 42	9.8	
G82.189-0.042	20 43 11.6	42 22 24	7.2	
G82.581+0.203	20 43 27.8	42 49 58	11.1	MSX6C G082.5828+00.2014
G82.571+0.194	20 43 27.9	42 49 11	11.1	

Notes. Displayed are an identifier equatorial coordinates radial velocity and a possibly related infrared source.

Most of the molecular outflows identified in this pathfinder project have an associated IRAS point source to pin-point the location of the young stellar object, but 18 of them do not (see Table 2). Owing to the complex nature of this region continuum surveys such as IRAS pick up everything along the line of sight making it hard to separate objects. Many of these outflows discovered in ^{12}CO(3–2) were found to overlap spatially with bright radio sources such as DR 17 and DR 23, but at very different velocities. Since IRAS is a continuum survey and has much poorer resolution than our ^{12}CO(3–2) data many IR sources that could be associated with these new outflows are lost through confusion with brighter more extended objects.

In Fig. 8 we display all outflows on an MSX image of the pathfinder area and on a zeroth moment map of the pathfinder ^{12}CO(3–2) survey over the velocity range from −20 km s^{-1} to +30 km s^{-1}. Outflow markers are colour coded to indicate their location within one of the three ^{12}CO(3–2) emission layers that we have identified in velocity space. There are only very few outflows at low positive velocities except for those likely related to the H II region complex NGC 6914. This indicates that there is little star formation related to the Cygnus Rift in the area of the pathfinder. Most outflows display negative velocities and are related to molecular clouds of bright ^{12}CO(3–2) emission that are dynamically connected to DR 21. The only exception is the previously mentioned cometary feature related to IRAS 20294+4255, which contains two molecular outflows. The outflows with a high positive radial velocity seem to be mostly related to DR 17, Cl 12, and Cl 14 (see Sect. 5.3).

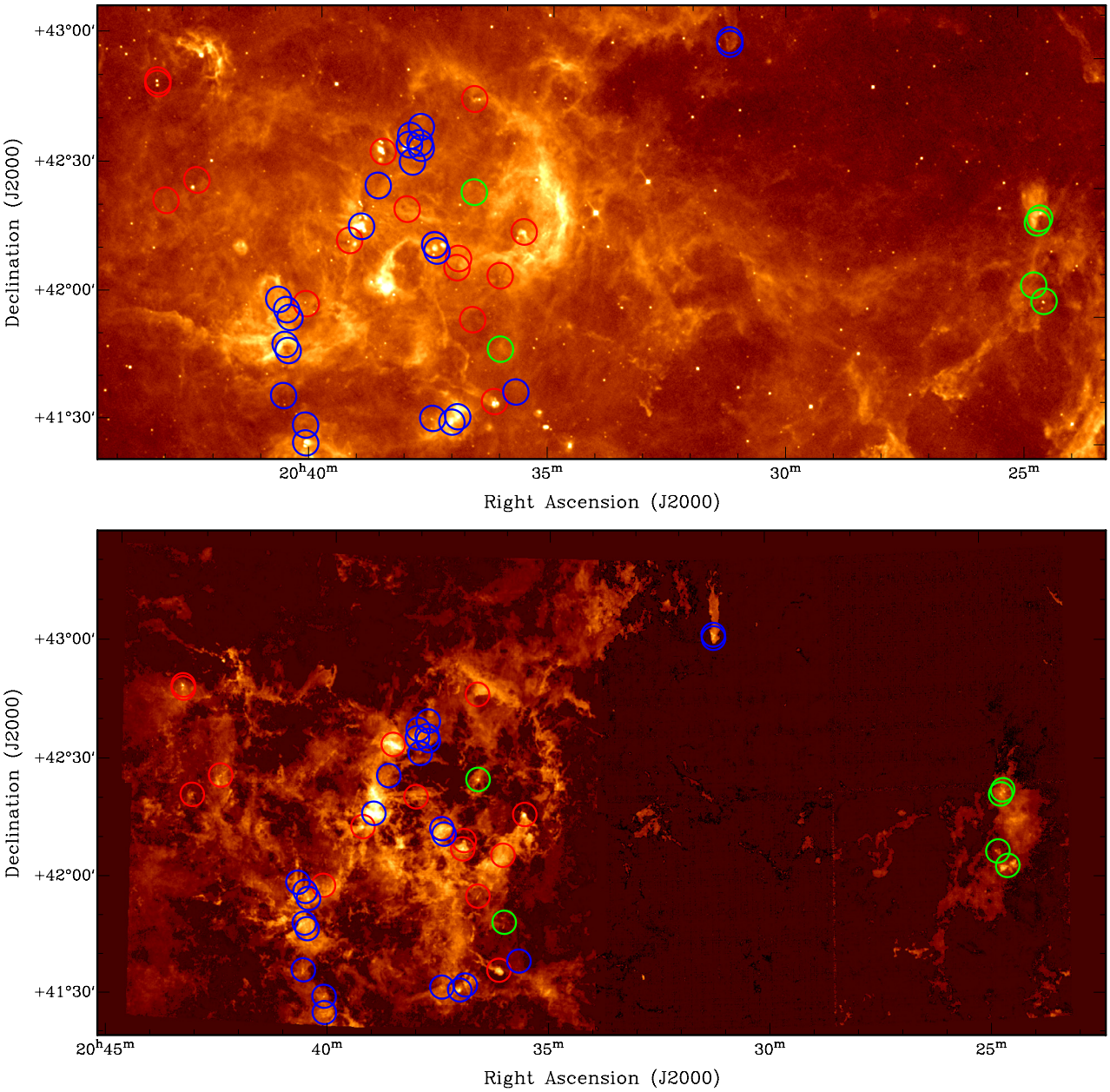

Fig. 8. MSX image at 8μ (*top*) and an integrated ^{12}CO(3–2) image (*bottom*), the zeroth moment map between −20 km s^{-1} and +30 km s^{-1} of the pathfinder area. The location of all 47 outflows that we detected are indicated. Blue circles indicate a negative radial velocity for the parent cloud of the outflow, green circles a connection with the Cygnus Rift (0 km s^{-1} $\leq v_{\rm rad} \leq$ 8 km s^{-1}, and outflows with velocities above 8 km s^{-1} for their parent cloud are marked by red circles.

As examples we display zeroth and first moment maps of two outflows related to IRAS 20294+4255 and IRAS 20227+4154 and their spectra in Figs. 9 and 10. The outflow lobes reveal themselves in the zeroth moment map as extended emission features, which have blue- or red-shifted velocities in their first moment maps. The blue- and red-shifted velocity wings are obvious in the emission spectra. The spectra of the bipolar outflow related to IRAS 20227+4154 also show a deep absorption line at about +6 km s^{-1} in both the red and blue-shifted spectra. This indicates that the outflow with its proto-star is not related to the large diffuse cloud overlapping with it, but must be located behind it.

A comparison of the optically thick ^{12}CO lines, J = 3–2 & J = 2–1, to the optically thin ^{13}CO lines, J = 3–2 & J = 2–1, was carried out by Choi et al. (1993) to investigate the optical depth in the line wings of molecular outflows. For the J = 3–2 lines they found that the optical depth decreases further into the line wings. The lowest velocity has the highest optical depth and physical parameters are underestimated when only the optically thick ^{12}CO line is used. This can be remedied with observations of the outflows in an optically thin line. A thorough study of a number of outflows detected in the pathfinder based on new JCMT observations of the more optically thin ^{13}CO(3–2) and C^{18}O(3–2) lines is being prepared and will soon be ready for publication.

5.3. Triggered star formation

A common occurrence around a stellar cluster containing massive stars is thought to be triggered star formation. Newly formed

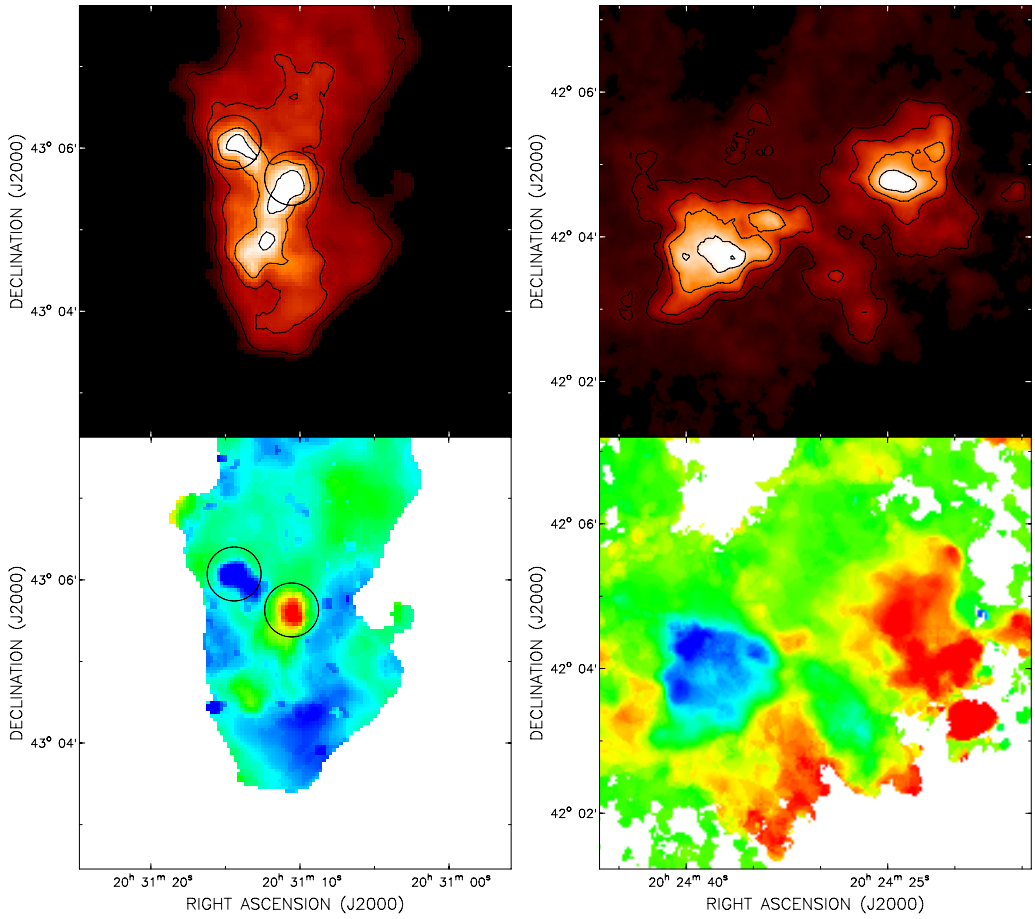

Fig. 9. Two examples of molecular outflows detected in the ^{12}CO(3–2) pathfinder. Zeroth moment maps are displayed in the top and first moment maps in the bottom. On the *left* we show the newly discovered outflow connected to IRAS 20294+4255 (black circles indicate the locations of the blue- and red-shifted lobes). The first moment map is displayed in the velocity range from −5 km s^{-1} (blue) to −0.5 km s^{-1} (red). On the *right* we show the large massive outflow connected to IRAS 20227+4154. The first moment map is displayed in the velocity range from +1.5 km s^{-1} (blue) to +8.5 km s^{-1} (red).

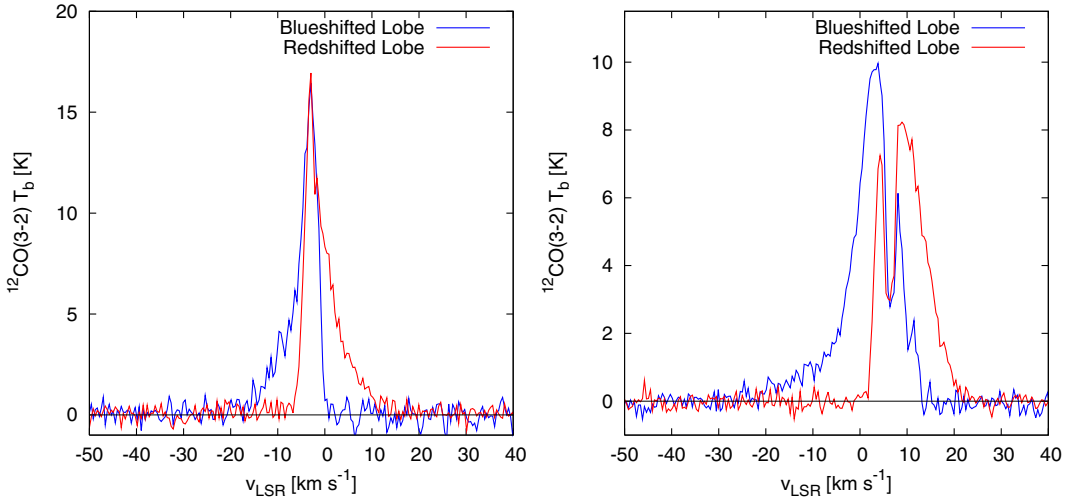

Fig. 10. Two examples of ^{12}CO(3–2) emission profiles towards the emission peaks of the blue-shifted and red-shifted lobes of the outflows connected to IRAS 20294+4255 (*left*) and IRAS 20227+4154 (*right*).

stars are often found in evaporating gas globules or *EGGs* (Hester & Desch 2005). These EGGs are located around the cluster's rim where the UV radiation from the cluster has had time to sweep up the local ISM and start to expose the young stellar objects within.

The pathfinder area is very close to the edge of the OB association Cyg OB 2 (Münch & Morgan 1953). From 2 MASS data Knödlseder (2000) finds that the Cyg OB 2 association more closely resembles a globular cluster with a population of around 2600 stars. He also finds that the diameter of Cyg OB 2 is around

4°, almost double the original estimate. This allows for the possibility that some embedded O- or B-type stars, not seen or not included in the original Cyg OB 2 association, are releasing large amounts of energy into the pathfinder area.

Two comet-shaped nebulae pointing exactly towards the centre of Cygnus OB2 are present in our ^{12}CO(3–2) pathfinder data. The large distances of these objects from the centre of Cyg OB2, one of them is over two degrees away, support the idea that the Cyg OB 2 association is larger than previously thought, although this is not conclusive evidence. Both cometary features contain molecular outflows. One of the cometary objects is related to IRAS 20294+4255 (see Figs. 9 and 10). It contains the outflows G 81.424+2.140 and G 81.435+2.147 (see Table 2) with a central velocity of about −2 km s^{-1}. This cometary cloud is located about 50 pc from the centre of Cygnus OB2 projected to the plane of the sky, assuming a distance of 1.7 kpc. The ^{12}CO(3–2) emission from this feature does not show any dynamical connection to DR 21 even though the radial velocity range is very similar. The other cometary feature pointing towards the centre of Cygnus OB2 contains outflow G 80.832+0.570 at a velocity of +11.5 km s^{-1} which seems to be related to IRAS 20343+4129. Whether there is a dynamical connection to W 75 N, DR 17, and connected molecular clouds, which have similar radial velocities, is not entirely clear.

It is interesting to note that the only cometary features in the pathfinder that seem to be connected to Cygnus OB2 show such a high difference in radial velocity. Clearly observations covering the entire area possibly influenced by Cygnus OB2 are required to solve this little mystery. With a bigger sample of cometary features connected to Cygnus OB2 we could map the entire area around this association in velocity space.

Another series of cometary nebulae in the pathfinder are found pointing to new cluster candidate Cl 14 and maybe Cl 12 (Le Duigou & Knödlseder 2002, see Fig. 11). These clusters overlap spatially with H II region DR 17 (Downes & Rinehart 1966), and are thought to be related to the Cyg OB 2 association. These cometary objects are the *pillars* from Schneider et al. (2006). No suitable UV radiation source had previously been identified that was able to cause their shape. Both of these clusters are proposed to be young clusters related to Cyg OB 2 with Cl 12 containing ∼37 OB stars and Cl 14 ∼12. Either cluster candidate should be able to supply the required radiation to expose these protostars. Furthermore, Cl 12 or Cl 14 may have caused the star formation seen in these cometary nebulae.

Several of these cometary features containing EGGs are pointing at Cl 14 (Fig. 11). These EGGs are likely the result of UV radiation from nearby stars dissociating and ionizing the outer layers of the molecular cloud. This warm gas is then blown away by stellar winds exposing the denser layers underneath. Gritschneder et al. (2009) have studied the effect that O-type stars have on the surrounding ISM. They find that as the ionization front from massive O stars penetrates deeper into the molecular cloud, gravitational instability is induced in the tips of the pillars, which leads to the production of protostars. The presence of multiple protostars around groups of O- or B-type stars cannot be a chance coincidence and thus provides direct evidence for triggered star formation. As the ionized gas expands through the molecular clouds it uncovers protostars. These protostars are still in the accreting phase, so as the UV radiation removes the molecular material around the protostar, a lower mass star will form. By studying the protostars formed in the EGGs around clusters and determining masses involved in the outflows we get an indication of whether or not these objects are being deprived of their molecular material (Hester & Desch 2005). Some

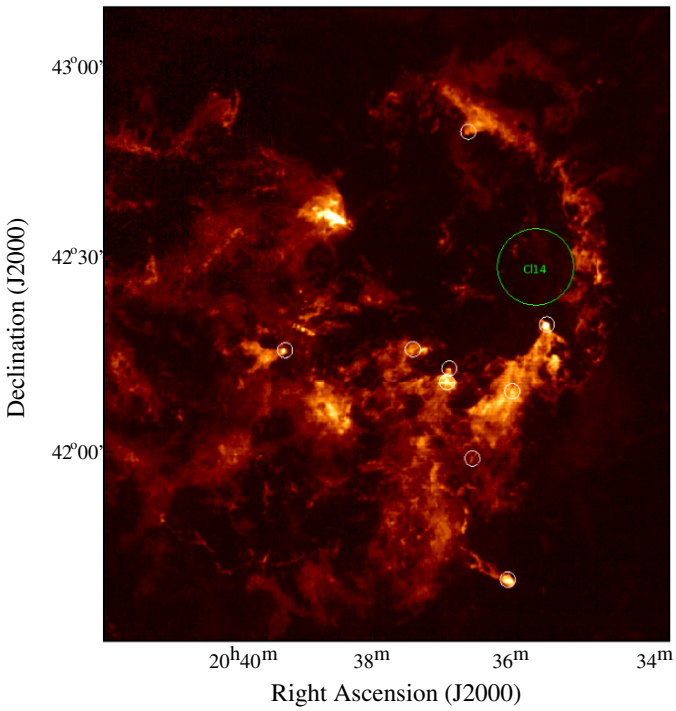

Fig. 11. Cometary features in a zeroth moment map of our pathfinder. The ^{12}CO3–2 emission was integrated from +10 to +25 km s^{-1}. Most cometary features point to the stellar cluster Cl 14 – which contains 12 OB-type stars – indicating triggered star formation.

of these objects could finish their accretion phase by the time the ionization front reaches the protostar. This depends on the nature of the UV source and the distance to the protostars. To accurately study the impact of strong UV sources on protostars a large sample of objects around various sources of strong UV radiation is required.

5.4. Overall structure of the Cygnus X region

Schneider et al. (2006) proposed that nearly all molecular clouds with radial velocities between −10 km s^{-1} and +20 km s^{-1} in Cygnus X form groups that are dynamically connected, and that most of the Cygnus X objects are located at the distance of the Cyg OB2 cluster at 1.7 kpc. With the information gathered in the pathfinder we will put the Schneider et al. postulate to the test.

There are only two objects/features in the Cygnus X region relevant for the pathfinder which have well determined distances and those are the Cygnus OB2 association at about 1.7 kpc and the Great Cygnus Rift between 500 and 800 pc (Schneider et al. 2006). The Great Cygnus Rift is represented in the pathfinder area by the low surface brightness molecular clouds in the ^{12}CO(3–2) emission layer at low positive velocities. The other two emission layers we found must be located behind the Cygnus Rift, simply because the Cygnus Rift is absorbing emission from all other molecular clouds. One example is shown in Fig. 6: the red-shifted high velocity wings of DR 21 are absorbed by the faint layer related to the Cygnus Rift. In addition we can see in Fig. 6 (bottom) that the ^{12}CO(3–2) emission in the blue-shifted high velocity wings related to W 75 N are not absorbed by the dense gas at negative velocity related to DR 21. This implies that W 75 N is closer to us than DR 21.

There is more evidence to support this. In Fig. 12 we display H I absorption profiles of bright radio sources in the pathfinder

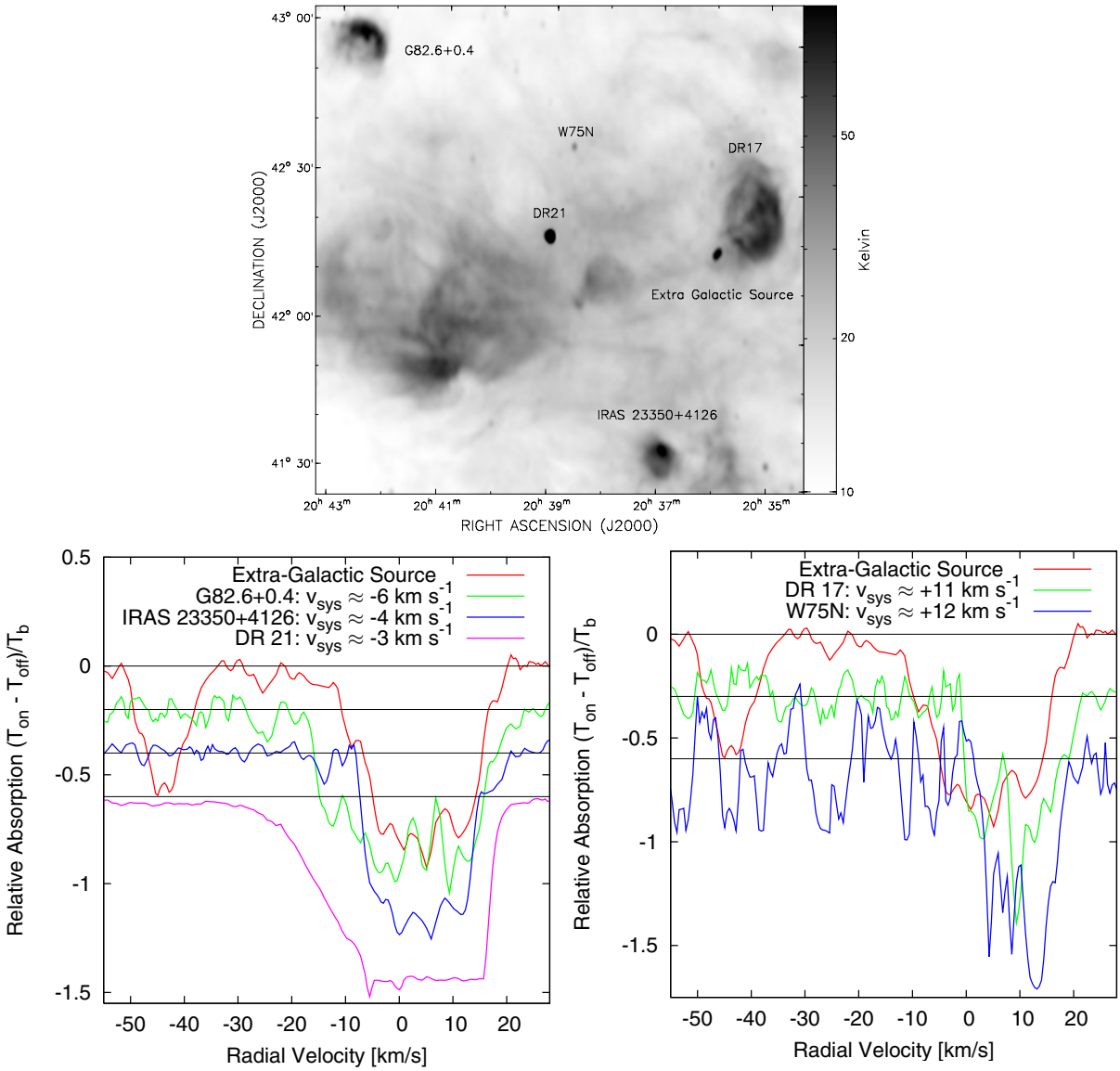

Fig. 12. Radio continuum image taken from the Canadian Galactic Plane Survey at 1420 MHz (*top*) and H I absorption profiles (*bottom*) of H II regions with high radio surface brightness in comparison with the profile of an extragalactic source. It is easy to see that the entire local H I absorbs the radio continuum emission from those H II regions with a negative systemic velocity $v_{\rm sys}$, while those with a high positive $v_{\rm sys}$ are only absorbed by a part of that gas, indicating that the negative-velocity H II regions are farther away than the high positive-velocity ones. This rules out the possibility of them being part of one big dynamically connected structure.

area and one nearby extragalactic source. The H I data were taken from the Canadian Galactic Plane Survey. The radio bright H II regions DR 21, IRAS 20350+4126, and G82.6+0.4 all seem to be related to ^{12}CO(3–2) emission at negative radial velocities in our pathfinder, while the H II regions DR 17 and W 75 N are related to molecular gas at high positive velocity. In addition we computed a H I absorption profile towards a presumed extragalactic source next to DR 17 (indicated in Fig. 12). The extragalactic source is the only source which shows an absorption component at about −45 km s^{-1}, confirming that its location must be well behind the other objects.

DR 21, G82.6+0.4, and IRAS 20350+4126 have absorption profiles similar to the extragalactic source at positive and low negative velocities. DR 21 seem to have a high velocity wing towards negative velocities, probably from dissociated and shocked molecular gas accelerated towards us. This kind of signal has previously been seen for other H II regions in the data of the Canadian Galactic Plane Survey before (Kothes & Kerton 2002). The sources with high positive radial velocities, DR 17 and W 75 N show only absorption components at high positive velocities, but nothing at low positive or negative velocities. This is another proof that the sources related to the ^{12}CO(3–2) emission layer at high positive velocities must be closer than those related to negative velocities. We demonstrated in Sect. 5.1 that both of these layers must have been pushed either towards us or away from us, but since the more positive layer is closer to us than the more negative one the source of the force that pushed those layers could not have been the same. This casts doubt on the proposed dynamical connection of most of the molecular clouds in Cygnus X.

Based on the information we have found in our data we propose the following order along the line of sight towards Cygnus X (as displayed in Fig. 13). We have the two fixed distances for the Cygnus Rift (500 to 800 pc) and Cygnus OB2 (1.7 kpc). Since the high positive-velocity material must be pushed away from us we believe its likely location is close to

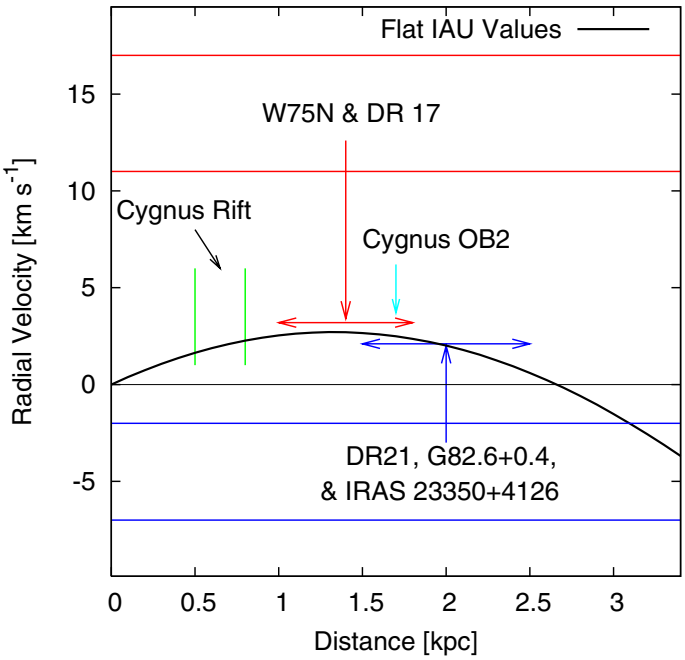

Fig. 13. Proposed locations of objects and emission layers along the line of sight as discussed in the text. The black line represents a flat rotation curve for the Galaxy with IAU supported values for $R_\odot$ and $v_\odot$.

the tangent point; there the energy required is lowest, because of the lower velocity difference. This is also in agreement with a location between the Cygnus Rift and the negative-velocity layer and a possible connection to DR 17 (Le Duigou & Knödlseder 2002). Our line of sight within the local spiral arm extends approximately to a distance of 2.5 kpc, as can be seen in the Milky Way model by Churchwell et al. (2009). We take this as an upper limit. The sources at negative velocity also have to be behind the highly positive layer and are therefore probably behind Cygnus OB2, although a connection cannot be ruled out.

6. Conclusions

The high critical density of the CO(3–2) transition makes it an excellent tracer of dense molecular material. This has allowed us to observe key stages in the molecule formation mechanism. We are currently able to qualitatively discuss the properties of the cold dense clouds making molecules, but a larger number of CO and HISA correlations needs to be observed in order to quantify the molecule formation rate. The Cygnus X region is also an excellent candidate for this type of survey as it provides multiple generations of star formation interacting at a relatively close distance from Earth. The nature of the CO(3–2) line makes it an excellent tool for discovering outflows. Of the outflows we detected more than 50% are new detections, and we have found all previously known outflows. In order to probe the outflow engine more observations of optically thin lines, for example ^{13}CO(3–2) and C^{18}O(3–2), need to be carried out. The detection of these outflows has provided direct evidence of sequential star formation. By studying all of these objects and the nature of their interaction with each other we can develop a deep understanding of the properties of these complex regions. Our pathfinder has only observed around 15% of the whole Cygnus X region. With the success of this survey one can only wonder what will come from a survey of the entire region.

Acknowledgements. The Dominion Radio Astrophysical Observatory is a National Facility operated by the National Research Council of Canada. The Canadian Galactic Plane Survey is a Canadian project with international partners, and is supported by the Natural Sciences and Engineering Research Council (NSERC). This research made use of data products from the Midcourse Space Experiment. Processing of the data was funded by the Ballistic Missile Defense Organization with additional support from NASA Office of Space Science. This research has made use of the NASA/ IPAC Infrared Science Archive, which is operated by the Jet Propulsion Laboratory, California Institute of Technology, under contract with the National Aeronautics and Space Administration.

References

Alves, J., & Homeier, N. 2003, ApJ, 589, L45
Bally, J., Reipurth, B., & Davis, C. J. 2007, in Protostars and Planets V, ed. B. Reipurth, D. Jewitt, & K. Keil, 215
Buckle, J. V., Hills, R. E., Smith, H., et al. 2009, MNRAS, 399, 1026
Burton, W. B. 1971, A&A, 10, 76
Choi, M., Evans, II, N. J., & Jaffe, D. T. 1993, ApJ, 417, 624
Churchwell, E., Babler, B. L., Meade, M. R., et al. 2009, PASP, 121, 213
Clark, J. S., Negueruela, I., Crowther, P. A., & Goodwin, S. P. 2005, A&A, 434, 949
Dent, W. R. F., Hovey, G. J., Dewdney, P. E., et al. 2009, MNRAS, 395, 1805
Downes, D., & Rinehart, R. 1966, ApJ, 144, 937
Gibson, S. J., Taylor, A. R., Higgs, L. A., Brunt, C. M., & Dewdney, P. E. 2005, ApJ, 626, 195
Glover, S. C. O., Federrath, C., Mac Low, M.-M., & Klessen, R. S. 2010, MNRAS, 404, 2
Gritschneder, M., Naab, T., Walch, S., Burkert, A., & Heitsch, F. 2009, ApJ, 694, L26
Hester, J. J., & Desch, S. J. 2005, in Chondrites and the Protoplanetary Disk, ed. A. N. Krot, E. R. D. Scott, & B. Reipurth, ASP Conf. Ser., 341, 107
Knödlseder, J. 2000, A&A, 360, 539
Knödlseder, J. 2004 [arXiv:astro-ph/0407050]
Kothes, R., & Dougherty, S. M. 2007, A&A, 468, 993
Kothes, R., & Kerton, C. R. 2002, A&A, 390, 337
Lada, C. J. 1985, ARA&A, 23, 267
Le Duigou, J.-M., & Knödlseder, J. 2002, A&A, 392, 869
Mao, Y., Wu, Y., & Liu, F. 2009, New Astron., 14, 391
Münch, L., & Morgan, W. W. 1953, ApJ, 118, 161
Piddington, J. H., & Minnett, H. C. 1952, Aust. J. Sci. Res. A Phys. Sci., 5, 17
Piepenbrink, A., & Wendker, H. J. 1988, A&A, 191, 313
Roberts, Jr., W. W. 1972, ApJ, 173, 259
Schneider, N., Bontemps, S., Simon, R., et al. 2006, A&A, 458, 855
Sofue, Y., & Reich, W. 1979, A&AS, 38, 251
Stahler, S. W., & Palla, F. 2005, in The Formation of Stars, ed. S. W. Stahler, & F. Palla (Wiley-VCH), 865
Taylor, A. R., Gibson, S. J., Peracaula, M., et al. 2003, AJ, 125, 3145
Wendker, H. J. 1984, A&AS, 58, 291
Wendker, H. J., Higgs, L. A., & Landecker, T. L. 1991, A&A, 241, 551
Wielen, R. 1979, in Stars and star systems, ed. B. E. Westerlund, Astrophys. Space Sci. Libr., 75, 81